Article:

Arfaie, A, Burns, AD, Dorrell, RM et al. (3 more authors) (2014) Optimised mixing and flow resistance during shear flow over a rib roughened boundary. International Communications in Heat and Mass Transfer, 58. 54 - 62. ISSN 0735-1933

https://doi.org/10.1016/j.icheatmasstransfer.2014.08.005

Optimised mixing and flow resistance during shear flow over a rib roughened boundary

A. Arfaie[a], A.D. Burns[a,1,*], R.M. Dorrell[b], J.T. Eggenhuisen[c], D.B. Ingham[a], W.D. McCaffrey[b]

[a]*Energy Technology and Innovation Initiative (ETII), University of Leeds, Leeds, LS2 9JT, UK*
[b]*School of Earth and Environment, University of Leeds, Leeds LS2 9JT, UK*
[c]*Department of Earth Sciences, Utrecht University, PO Box 80021, 3508 TA Utrecht, Netherlands*

Abstract

A series of numerical investigations has been performed to study the effect of lower boundary roughness on turbulent flow in a two-dimensional channel. The roughness spacing to height ratio, w/k, has been investigated over the range 0.12 to 402 by varying the horizontal rib spacing. The square roughness elements each have a cross-sectional area of $(0.05H)^2$, where H is the full channel height. The Reynolds number, Re_τ is fixed based on the value of the imposed pressure gradient, dp/dx, and is in the range $6.3\times10^3-4.5\times10^4$. A Reynolds Averaged Navier-Stokes (RANS) based turbulence modelling approach is adopted using a commercial CFD code, ANSYS-CFX 14.0. Measurements of eddy viscosity and friction factor have been made over this range to establish the optimum spacings to produce maximum turbulence enhancement, mixing and resistance to flow. These occur when w/k is approximately 7. It is found that this value is only weakly dependent on Reynolds number, and the decay rate of turbulence enhancement as a function of w/k ratio beyond this optimum spacing is slow. The implications for heat transfer design optimisation and particle transport are considered.

Keywords: Turbulent flow, Roughness, CFD

1. Introduction

The study of turbulent flow over surface roughness is important in a variety of engineering and environmental applications. Surface roughness is used as a tool to enhance heat transfer in turbines [1], heat exchangers [2], micro-scale electric mechanical systems [3], the hypervapotron (high heat flux) heat transfer device employed in nuclear fusion [4], chemical reactors, refrigeration systems and air conditioners [5]. Examples of rough-wall flows include particle transport in pipes and channels with rough walls, supersonic flows inside cavities for aerospace applications, wind flow over urban-like surfaces and turbidity currents over rough substrates [1, 6–9]. In recent decades, a wide range of experimental and computational studies has been performed to understand the effect of surface roughness on the structure of the turbulent flow. The computational domain and experimental configuration of these studies are typically a two-dimensional or three-dimensional rectangular channel flow with roughness on one or both walls [10–23]. The effect of surface roughness on the flow, as reviewed by Jimenez [24] and more recently by Antonia and Djenidi [25], is often separated into three different regimes. Chow [26] was first to identify three flow regimes over beam-type roughness as quasi-smooth or skimming flow, wake-interference flow and isolated-roughness flow. Perry et al. [27] categorised two distinct types of roughness, namely, "d" and "k" denoting channel height and roughness height, respectively (see below), following from the earlier experimental work conducted by Nikuradse [28] on the turbulent flow of fluids in rough pipes.

The roughness type can be correlated to the spacing to height ratio of a roughness element, w/k. The roughness spacing is differently defined as either the distance between roughness faces w, or the distance between roughness-element center-lines λ; values differ by unity for square ribs. Therefore one must be careful not to confuse the cavity width to height ratio w/k to the pitch to height ratio λ/k.

For a sufficiently low width to height ratio, $w/k \lesssim 2$, or d-type roughness, the flow undergoes a "skimming flow" regime and the effective height, y_l above the chan-

*Corresponding author.
Email address: a.d.burns@leeds.ac.uk (A.D. Burns)

Nomenclature

$\frac{\partial p}{\partial x}$	mean pressure gradient
$\overline{\acute{u}_i \acute{u}_j}$	Reynolds stress
p_0	reference pressure point
Greek Variables	
ε	dissipation rate of K
μ	dynamic viscosity
μ_{eff}	effective viscosity
μ_t	turbulent viscosity
ν, ν_t	Kinematic viscosity, eddy viscosity
ρ	density
τ_w	wall shear
ω	turbulent eddy frequency
Roman Variables	
C_f	skin friction coefficient$\left(= \frac{\tau_w}{\frac{1}{2}\rho \overline{U}_b^2}\right)$
C_p	pressure coefficient $\left(= \frac{p-p_0}{\frac{1}{2}\rho \overline{U}}\right)$
f	Darcy friction factor $\left(= \frac{(H/2)(dp/dx)}{0.5\rho \overline{U}^2}\right)$
H	full channel height
K	Turbulence Kinetic Energy
k	roughness height
k^+	Dimensionless roughness height $\left(= \frac{k u_\tau}{\nu}\right)$
p	pressure
Re_τ	$u_\tau(H/2)/\nu$, shear Reynolds number
Re_b	$U_b(H/2)/\nu$, bulk Reynolds number
u_τ	shear velocity $\left(= \sqrt{\tau_w/\rho}\right)$
U_b	bulk velocity
w	width of the cavity
x	streamwise direction
y	wall-normal direction
y^+	non dimesnional distance to the wall $\left(= \frac{y u_\tau}{\nu}\right)$
y_l	The origin of the logarithmic profile
Subscripts	
i, j	coordinate direction 1,2 or 3
max	maximum of variable
min	minimum of variable
rms	root mean square value of the variable

nel bed where the velocity profile begins to take a logarithmic shape becomes independent of the roughness height, k. In this flow regime there is minor shedding or interaction from the vicinity of the roughness element to the outer flow region [22, 29, 30]. The k-type roughness (isolated-roughness flow regime) is associated with $w/k \gtrsim 4$. The roughness height becomes a crucial parameter for $w/k \gtrsim 4$ when the flow in the roughness cavity begins to interact with the main body of the flow. For this roughness type, the origin of the logarithmic profile, y_l is proportional to the roughness height, k and the flow regime is characterised by separation occurring at the crest of the first roughness element followed by a reattachment within the distance away from the next adjacent element. The experimental study of Djenidi et al. [22] suggested a similarity in the quasi streamwise vortices and low-speed streaks of the roughened wall cases, to a flat turbulent boundary layer. Tani [31] found the demarcation line between the $d-$type and the $k-$type roughness occurs at $w/k = 4$. Cui et al. [16] observed a similar transition for $w/k = 4$ and named this roughness type as intermediate. This transition flow regime corresponds to with the wake interference flow regime classified by Chow [26]. In this regime a weak interaction between the inner and outer roughness layer occurs and the reattachment takes place at the crest of the next roughness element. The direct numerical simulation (DNS) of Leonardi et al. [29] showed that the intermediate regime appears within the range $3 < w/k < 7$.

In a fully rough flow, the ratio of the product of the roughness height and shear velocity to the kinematic viscosity of the fluid k^+ ($k^+ = k u_\tau/\nu$), is greater than ≈ 70 and the pressure drag component of the total drag dominates the viscous drag component. In this flow regime the flow characteristics are only dependent on the roughness spacing to height ratio w/k. Hence, the viscous length scale (ν/u_τ) near the wall scale becomes irrelevant [20, 32].

Orlandi et al. [33] and Leonardi et al. [30] found similarity in the vortex shedding distribution between the intermediate and k-type roughness. Therefore, they suggested that classification of different roughness types should not be based on the state and intensity of vortex shedding. Instead, they related the transition between d-type and k-type to the magnitude of the viscous and pressure drags.

Both LES and DNS numerical modelling of rough-wall flows have proven to be highly accurate in predicting the turbulent kinetic energy and Reynolds stresses in the near-wall region. However, in order to capture most of the flow characteristics within the roughness sub-layer, a higher grid resolution and time step accuracy is required than in a normal smooth-wall case. This makes such approaches expensive, particularly for high Reynolds number flows. Leonardi et al. [29] used DNS to investigate the effect of the w/k ratio on the turbulence structure near the wall, and its overlying flow by considering two-point velocity correlations. They observed that in the fully rough regime, with the increase in the w/k ratio, the coherence structure becomes less elongated in the streamwise direction, and larger in the spanwise direction as a result of outwards jets of fluid at the leading edge of the roughness element. Such coherence structure would appear to be less influenced by the rough wall in the transition regime ($k^+ \simeq 13$), as observed by Ashrafian et al. [34]. The maximum strength of the outward jet and the minimum reduction of the coherence occurred at the critical value $w/k = 7$. They further found that the influence of roughness can extend up to $2k$ above the roughness crest for $w/k = 3$ and up to $5k$ for $w/k = 7$. The study conducted by Cui et al. [16], for a channel with transverse rib roughness on one wall, suggests a strong interaction between the inner and outer layer roughness for k-type roughness.

Numerous authors have performed numerical and experimental analyses to investigate the relationship between heat transfer and fluid flow behaviour by varying the w/k ratio [35–38]. However most of these investigations suffer from a lack of a detailed range of w/k ratio and Reynolds number. The most detailed study was performed experimentally by Furuya et al. [39] and Okamoto et al. [40] for boundary layer fluid flow. Furuya et al. [39] investigated the maximum resistance of the turbulent boundary layer in a plate roughened by equally spaced wires. They found that the maximum skin drag coefficient, c_f and pressure coefficient, c_p values appears at $w/k = 7$. However the DNS result of Leonardi et al. [29] suggests that minimum c_f occurs at $w/k = 7$, but agrees with the maximum pressure coefficient c_p occurring at this w/k ratio. The experimental study by Okamoto et al. [40] has shown that the maximum heat transfer occurs when the turbulence intensity is maximised. They have shown that the maximum flow resistance occurs between $w/k = 6$ and $w/k = 8$. This paper aims to explicitly identify where the optimum flow resistance occurs for a more detailed range of w/k ratio as a function of Reynolds number.

In the present study, we employ a RANS method to simulate turbulent flow in a two-dimensional channel with an asymmetric two-dimensional rough lower boundary for a wide range of ratio w/k and Reynolds numbers. In this paper, we attempt to accurately constrain the critical w/k ratio for an optimum turbulence enhancement, mixing and resistance to the flow. For this purpose, we evaluate the dependence of eddy viscosity and friction factor on Reynolds number for a series of w/k values. The aims of this research are to better constrain optimum conditions for heat transfer, and to assess lower boundary roughness effects on turbidity current turbulence generation, flow depletion and runout.

The paper is organized as follows. Sections 2 and 3 give brief description of the numerical procedure and flow configuration. In Section 4 we validate our model with previous experimental and numerical data. The results of the numerical modelling are given in Section 5 and discussed in Section 6.

2. Numerical method

2.1. Turbulence modelling

Steady state CFD simulations have been performed using the commercial code, ANSYS CFX 14.0. This code uses a finite volume method to solve the Reynold time averaged Navier-Stokes equations by a coupled solver. Furthermore, the fluid is assumed to be incompressible and Newtonian. Numerous turbulence models were employed for comparisons against experimental and numerical results in literature. The Shear Stress Transport (SST) turbulence model was identified as the model of choice, motivated by the work of Milnes et al. [4] on deep cavities. This model uses "Automatic Near Wall Treatment", which switches between the low-Re formulation and wall function depending on the resolution of the mesh near the wall [41–43]. Other turbulence modelling choices included, $K - \varepsilon$ and Reynolds stress turbulence models. The $K - \varepsilon$ standard model uses a scalable wall function to avoid problems in resolving grid points in the viscous layer [41]. These models have been used extensively, and have been shown to be reliable in terms of robustness and accuracy [42, 44]. The Reynolds stress models are not based on the eddy viscosity hypothesis but instead directly solve the transport equation for the individual stress components per time step. The BSL Reynolds stress model is an ω-based Reynolds stress model whereas the LRR and SSG

Reynolds stress models are ε-based models. The BSL and LRR Reynolds stress models use a linear pressure-strain correlation while SSG uses a quadratic relation [41, 45, 46].

In total, 28 geometries with varying width to roughness height ratio have been meshed using the Hexa mesh method as employed in ANSYS ICEM. A preliminary mesh independence study was carried out in order to verify that the solution is grid independent. The first wall node was positioned at $y^+ \approx 1$ for the SST model and at least 15 further nodes were placed inside the boundary layer in order to resolve the viscous layer. The variable y^+ is the dimensionless distance which is based on the the height of the first node from the wall and wall shear stress (yu_τ/ν). For models that use the scalable wall function, at least 10 nodes were placed in the boundary layer in the direction normal to the wall to achieve $y^+ \approx 11$. A residual target of 1×10^{-6} was chosen, as the convergence criterion for all the quantities and simulations.

2.2. Governing equations

The mathematical equations for steady Reynolds averaged models are based on conservation of fluid mass, continuity and momentum as follows:

Continuity:

$$\frac{\partial \overline{U}_i}{\partial x_i} = 0 \tag{1}$$

Momentum:

$$\frac{\partial}{\partial x_j}\left(\rho \overline{U}_i \overline{U}_j\right) = -\frac{\partial \overline{p'}}{\partial x_i} + \frac{\partial}{\partial x_j}\left[\mu_{eff}\left(\frac{\partial \overline{U}_i}{\partial x_j} + \frac{\partial \overline{U}_j}{\partial x_i}\right)\right] + S_M \tag{2}$$

$$\overline{p'} = \overline{p} + \frac{2}{3}\rho K + \frac{2}{3}\mu_{eff}\frac{\partial U_k}{\partial x_k} \tag{3}$$

where $\overline{p'}$ is the time-averaged modified pressure as defined in equation (3), S_M is the sum of the body forces, and $\mu_{eff} = \mu + \mu_t$, the effective viscosity is the sum of the fluid, μ and turbulent viscosity mu_t. The turbulent viscosity is given in standard form as,

$$\mu_t = C_\mu \rho \frac{K^2}{\varepsilon} \tag{4}$$

For the Reynolds stress turbulence models, steady Reynolds averaged momentum equations are given by,

$$\frac{\partial}{\partial x_j}\left(\rho \overline{U}_i \overline{U}_j\right) - \frac{\partial}{\partial x_j}\left[\mu\left(\frac{\partial \overline{U_i}}{\partial x_j} + \frac{\partial \overline{U_j}}{\partial x_i}\right)\right] = -\frac{\partial \overline{p''}}{\partial x_i} - \frac{\partial}{\partial_j}\left(\rho \overline{u_i u_j}\right) + S_{M_i} \tag{5}$$

In contrast to the eddy viscosity model, the modified pressure, $\overline{p''}$ used in momentum equation (5), has no turbulence contribution and is written as a function of static pressure as,

$$\overline{p''} = \overline{p} + \frac{2}{3}\mu_{eff}\frac{\partial \overline{U}_k}{\partial x_k} \tag{6}$$

The standard Reynolds stress turbulence models use the ε-equation and instead solve the transport differential equation individually for each Reynolds stress component. The Reynolds stress transport equations for steady flow are given as follows:

$$\frac{\partial}{\partial x_k}\left(\overline{U_k}\rho \overline{u_i u_j}\right) - \frac{\partial}{\partial x_k}\left[\left(\mu + \frac{2}{3}C_s \rho \frac{K^2}{\varepsilon}\right)\frac{\partial \overline{u_i u_j}}{\partial x_k}\right] = \overline{P_{ij}} - \frac{2}{3}\delta_{ij}\rho\varepsilon + \Phi_{ij} \tag{7}$$

$$\overline{P_{ij}} = -\rho\overline{u_i u_k}\frac{\partial \overline{U_j}}{\partial x_k} - \rho\overline{u_j u_k}\frac{\partial \overline{U_i}}{\partial x_k} \tag{8}$$

where C_S is a constant, Φ_{ij} is the pressure-strain correlation, and P_{ij} is the production term.

Both the $K - \varepsilon$ and $K - \omega$ models use the eddy viscosity hypothesis, which is described using the following formula for the Reynolds stresses in incompressible flows:

$$\overline{\acute{u}_i \acute{u}_j} = \frac{2}{3}K\delta_{ij} - \mu_t\left(\frac{\partial \overline{U_i}}{\partial x_j} + \frac{\partial \overline{U_j}}{\partial x_i}\right) \tag{9}$$

Hence the 2D assumptions in the RANS simulations are given by:

$$\overline{\acute{u}^2} = \frac{2}{3}K - 2\mu_t\frac{\partial \overline{u}}{\partial x} \tag{10}$$

$$\overline{\acute{v}^2} = \frac{2}{3}K - 2\mu_t\frac{\partial \overline{v}}{\partial y} \tag{11}$$

$$\overline{\acute{w}^2} = \frac{2}{3}K \tag{12}$$

Whilst we constrain the flow next to a wall to a two-dimensional problem, it is to be noted that $\overline{\acute{w}^2} \neq 0$ in equation (9) and the model still accounts for 3D fluctuations. If $\left(\overline{\acute{u}^2}, \overline{\acute{v}^2}\right)$ are both measured experimentally, it is possible to deduce K. For incompressible flows, $\partial\overline{v}/\partial y = 0$ and this gives,

$$K = \frac{3}{4}(\overline{\acute{u}^2} + \overline{\acute{v}^2}) \tag{13}$$

In equation (13), the value of the turbulent kinetic energy K can be compared with the predicted results for the $K-\varepsilon$ and $K-\omega$ models. In addition, if only the $\overline{\acute{u}^2}$ measurements are available, then equation (13) is used to deduce $\overline{\acute{u}^2}$ from the $K-\varepsilon$ and $K-\omega$ predictions. However, if a Reynolds stress model is used then $(\overline{\acute{u}^2}, \overline{\acute{v}^2}, \overline{\acute{w}^2})$ are computed automatically and thus, in contrast, the values are less difficult to obtain.

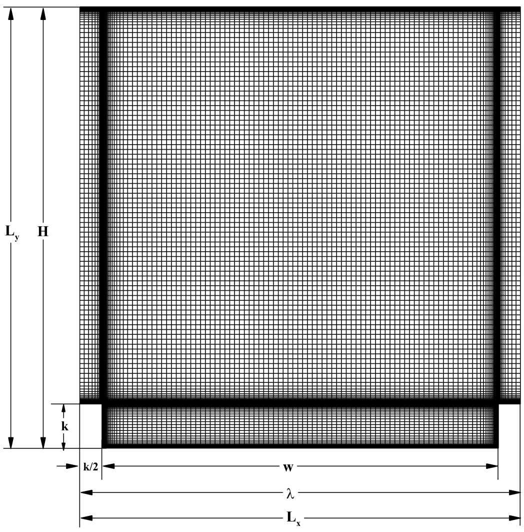

Figure 1: Computational domain and hexahedral grid system of the channel flow with surface roughness showing the parameters for $w/k = 9$.

3. Flow configuration

Figure 1 shows the computational domain with its coordinate system and the roughness element shape. The domain size is $\left(L_x, L_y\right) = (w/k + k, H)$. The roughness element is in a non-staggered, two-dimensional transverse square arrangement, with a cross section $k \times k$, positioned on the lower boundary. Periodic boundary conditions are used in the streamwise direction and a symmetry condition is applied in the spanwise direction. A no-slip boundary condition was applied to the upper and lower wall. A mean pressure gradient is imposed as a source term in the U-momentum equation. The Reynolds number is determined based on u_τ and half-channel height, $Re_\tau = (H/2)\, u_\tau/\nu$. The width-to-height ratio w/k was varied from 0.12 to 402 (0.12 , 0.27 , 0.51 , 0.75 ,1 ,2 ,3 ,4, 5, 6 , 7 ,8 , 9 , 10 , 11, 12, 18, 24, 30, 42, 54, 63, 75, 87, 96, 204, 300, 402). Turbulent flow over surface roughness can experience either a hydraulically smooth wall regime, a transitional-roughness regime, or a fully rough flow regime depending on the value of k^+(hydraulically smooth wall: $0 \lesssim k^+ \lesssim 5$, transitional-roughness regime: $5 \lesssim k^+ \lesssim 70$ and fully rough flow: $k^+ \gtrsim 70$). For the original simulations reported here, the roughness element height is $0.05H$, where H is the channel height, and the dimensionless roughness height, and the dimensionless roughness height is in the range of the fully rough regime, $k^+ \geqslant 70$. The simulations have been performed for 28 domains for values of dp/dx, 1×10^{-4}, 5×10^{-4}, 1×10^{-3}, 2×10^{-3}, 3×10^{-3}, 4×10^{-3} and 5×10^{-3} $kgm^{-2}s^{-2}$.

4. Validation

In order to validate the solution, the experimental results of Okamoto et al. [40], Djenidi et al. [22] and the LES of Cui et al. [16] are compared to the present data. In this work, the computational geometry is set to match that of Cui et al. [16], i.e., $0.1H$. The mean pressure gradient, dp/dx is varied to obtain the Reynolds number, Re_b close to the experimental and LES data.
The Figures 2 (a)-(d) show the streamwise velocity profiles normalised by the maximum streamwise velocity obtained from the turbulence model solutions for $w/k = 1, 4, 8, 9$. The velocity profiles are displayed with a line located at the centre of the channel in the cavity from the upper to the lower wall boundaries. Overall for all the turbulence models, the velocity profiles overall show a reasonable agreement with the previous numerical and experimental data. The $K-\varepsilon$ model shows the best agreement compared to the available data. To further support this validation, the present $K-\varepsilon$ model has been compared to the experimental data for $w/k = 8$ and $w/k = 9$, respectively in figure 2 (c) and 2 (d).

Figure 2 shows a more pronounce resistance effect near the roughness element as the spacing between the roughness element increases. This leads to the up-lifting of the U_{max} towards the upper flat wall. This effect is more apparent for $w/k = 8$ and $w/k = 9$.

Figure 3 shows the wall pressure drag distribution along a line positioned at the bottom of the cavity for $w/k = 9$. This distance is normalised by the roughness height "k" and K-ε model is tested for validation. The agreement between the C_p computation and LES of Cui et al. [16] is satisfactory. The zero pressure drag due to

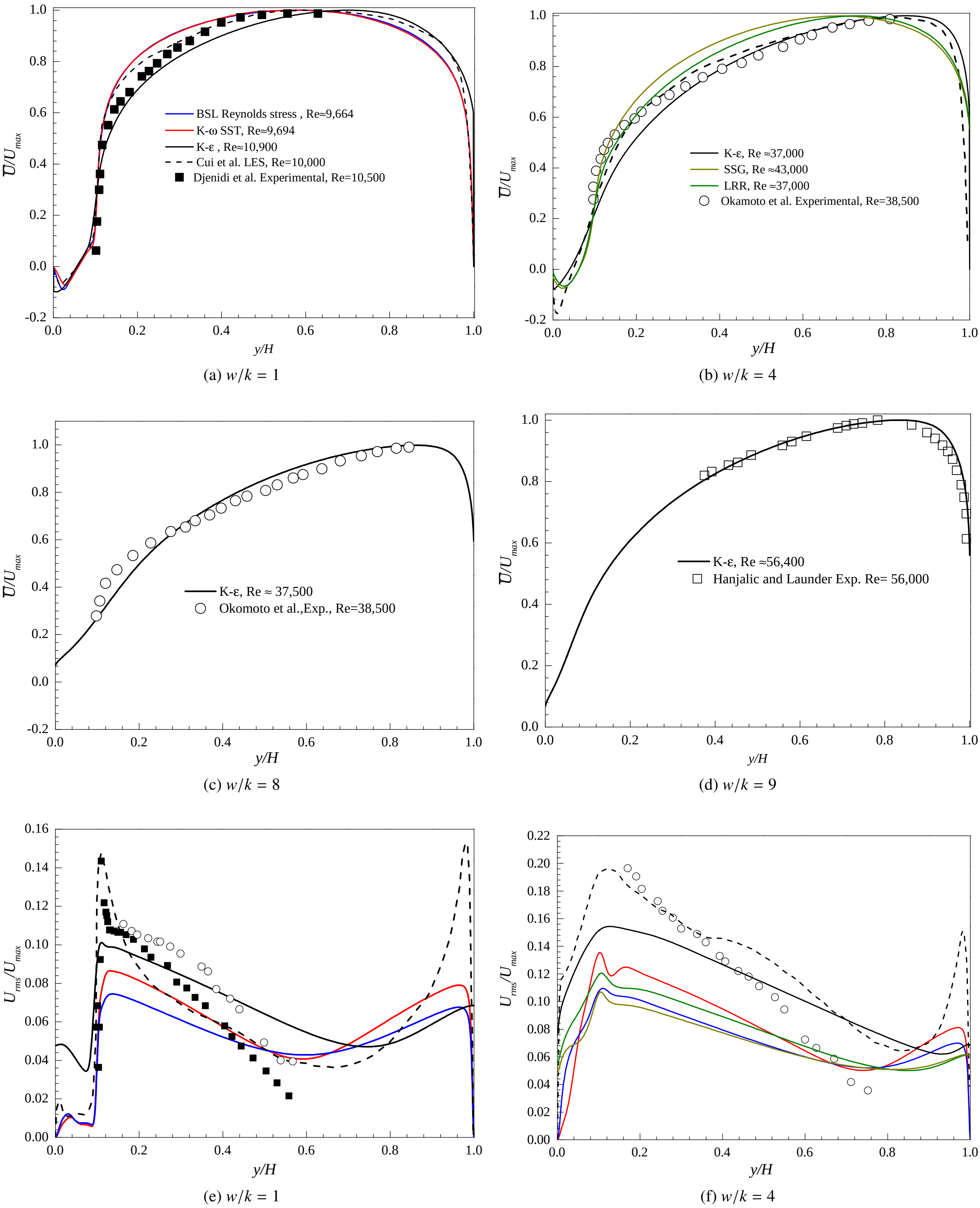

Figure 2: Plots of the computed velocity profiles of various turbulence models on the centre line of the channel for (a) $w/k = 1$, (b) $w/k = 4$, (c) $w/k = 8$ at $Re \approx 56,000$ (d) $w/k = 9$ at $Re \approx 37,000$ and (e) Turbulence intensity at $w/k = 1$ (f) Turbulence intensity at $w/k = 4$, with the result of Hanjalic and Launder [47], Okamoto et al. [40], Djenidi et al. [22] and LES of Cui et al. [16].

the recirculation region at the back face of the rib predicted by the $K - \varepsilon$ model shows a close resemblance to that obtained with the LES result. The pressure coefficient is defined as

$$C_p = \frac{p - p_0}{\frac{1}{2}\rho\overline{U}} \tag{14}$$

The normalised streamwise turbulence intensity U_{rms} at the centre of the cavity is also compared for $w/k = 1, 4$ with previous experimental and numerical data in figure 2. The streamwise turbulence intensity U_{rms} is defined by $\left(\sqrt{\acute{u}_i\acute{u}_j}\right)$, which is the root mean square of the Reynolds stress uu, $R_{ij} = -\rho\overline{\acute{u}_i\acute{u}_j}$, normalised by the maximum velocity, U_{max}. The normalised turbulence intensity results are more sensitive and show discrepancies. As illustrated by figure 2 (e)-(f), RANS model show poor prediction of the turbulence intensities for both $w/k = 1$ and $w/k = 4$. On the other hand, the discrepancies for the standard $K - \varepsilon$ model appear to be less severe than those of the other RANS models.

The $K - \varepsilon$ turbulence model demonstrates a reasonable prediction in capturing velocity profiles. Therefore, the predictions of the eddy viscosity must be reasonably accurate, as the influence of turbulence on the flow field is largely governed by the eddy viscosity term in equation (2). Moreover, turbulent dispersion of heat and small particles may be modelled using an eddy diffusivity which is proportional to the eddy viscosity. Therefore, the the $K - \varepsilon$ model has been used to further examine the characteristics of the roughened wall flow over a range of aspect ratios.

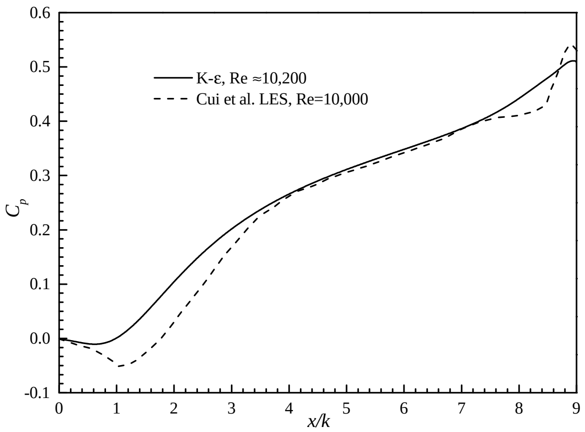

Figure 3: The pressure coefficient profile at $w/k = 9$.

5. Results

In total, 196 RANS modelling simulations were performed to study turbulent flow over two-dimensional square roughness elements for various Reynolds numbers and w/k ratios. The w/k ratio lies between 0.12 and 402 while the Reynolds number range from $6.3 \times 10^3 - 4.5 \times 10^4$. The streamlines and reattachment length of the averaged two-dimensional velocity field of the results are presented. The flow is over form-type roughness as the ratio of the boundary layer thickness to the roughness height is smaller than the critical value, $\delta/k \lesssim 80$ as suggested by Jimenez [24]. Thus, the viscous effect of the wall will be negligible relative to the pressure drag produced by the rib.

The trend in which the velocity profile $\overline{U}/U_{max}$ changes has been examined with respect to Reynolds number for different classes of rough wall. The results are compared with the effect of Reynolds number on a typical turbulent layer profile over a flat plat. The direction in which the velocity profile changes as a result of increase in Reynolds stresses through a rise in perpendicular mass interchanges between inner and outer fluid layers. The direction in which the velocity profile changes for the $d-$type is similar to flow in flat plates. However, it is interesting to note that this change occurs at a lower rate compared to flat cases. Two interesting observation can be made for $w/k = 3$ and $w/k = 4$ velocity profiles. Firstly,the effect of Reynolds number appears to be insignificant for intermediate type roughness. Secondly, the direction of the velocity change is seen to reverse towards the flow. The trend for $k-$type roughness has previously been extracted by Hanjalic and Launder [47] and Leonardi et al. [48] which agrees with the present study. The key point to take away from this comparison is the critical transition point in terms of Reynolds number effect, the ratio $w/k = 3$, between $d-$type and $k-$type.

Finally, to further characterise the bed roughness, flow resistance and eddy viscosity variation are evaluated. The dependence of these results on the Reynolds number as a function of width-to-height ratio will be discussed.

5.1. Reattachment length and streamlines

Two-dimensional mean velocity streamlines are created to illustrate the flow distribution in the inner and outer roughness element. In this section effect of the w/k variation on the flow pattern is considered. The separation and reattachment region shown in figure 4 for different roughness type is similar to the flow behaviour observed by Cui et al. [16] and Leonardi et al. [30].

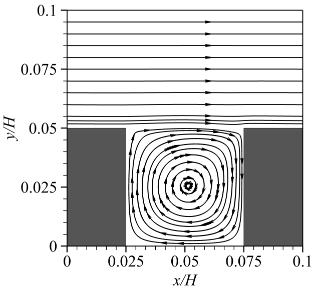

(a)

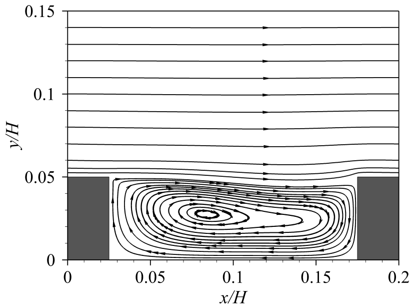

(b)

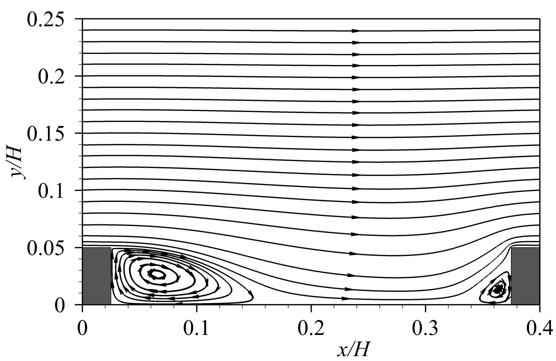

(c)

Figure 4: Distribution of mean streamlines velocity for (a) $w/k = 1$, (b) $w/k = 3$, (c) $w/k = 7$.

Separation-reattachment region are developed for all the modelled w/k ratios. Figure 4 shows the change in flow pattern from $w/k = 1$ to $w/k = 7$. The vortices are seen to become elongated from $w/k = 1$ to $w/k = 4$ and the reattachment still occurs at the leading edge of the neighbouring element as shown in figures 4(a)-(b). As the w/k ratio increases further the vortices stretch until they split and the flow reattaches on the lower boundary between adjacent roughness elements, as observed in figure 4(c). Ashrafian et al. [34] found that in the transitionally rough flow regime at $w/k = 7$, the apparent reattachment does not occur at the channel bed. However, Leonardi et al. [21] reported that for $w/k = 7$, in the fully rough regime, the flow reattaches on the bottom of the channel between the roughness elements. In the transitionally rough regime the flow become dependent on the Reynolds number [49] and therefore the reattachment location may become sensitive to the roughness height.

The reattachment location is determined by zero non-dimensionalised wall-shear stress for a selection of w/k ratios where the reattachment occurs at the cavity, as shown in figure 5(a). The distance x_r is measured from the step and normalised by the roughness height, k. Figure 5(a) shows that the value of reattachment length increases with an increase in the ratio, w/k. The reattachment point for each of the selective w/k ratios is plotted and a quadratic polynomial curve can be fitted to the data, as illustrated in figure 5(b).

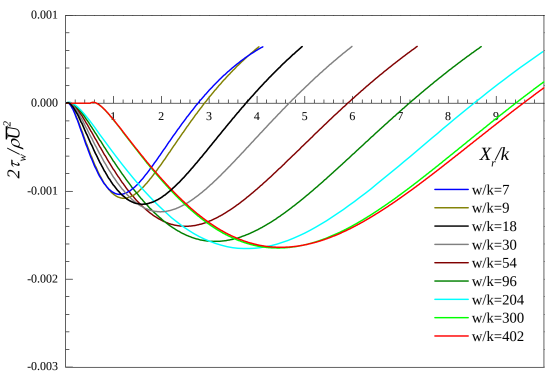

(a)

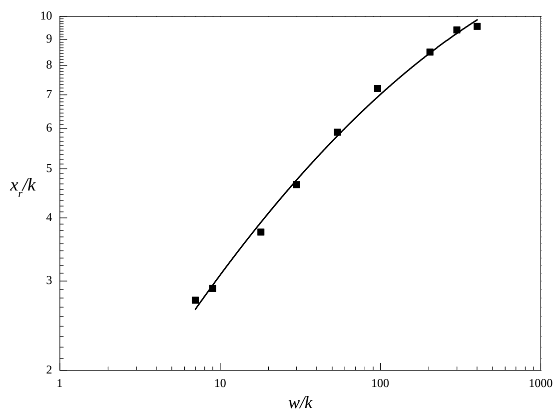

(b)

Figure 5: (a) The normalised wall shear stress versus the normalised distance between the adjoining ribs and (b) Graph of the reattachment point with varying the width-to-height ratio.

5.2. Flow resistance

The loss of energy from a flow needed to overcome a rugose surface is commonly evaluated using the skin-friction drag and form drag which sum to the total drag. The ratio of the form drag to skin drag increases with the w/k ratio. The friction factor for the turbulent flow structure obtained near the roughness element is a function of the ratio w/k and the Reynolds number, Re_τ. Since the value of the form drag for higher values of the ratio w/k is significantly greater than the value of the skin-frictional drag, then the entire flow resistance as a function of w/k occurs in the form of the pressure drag. The Darcy friction factor equation is defined as

$$f = \frac{(H/2)\,(-dp/dx)}{0.5\rho \bar{U}^2} \tag{15}$$

where dp/dx is the main driving force against the wall shear stress τ_w and $\overline{U}$ is the area-weighted average streamwise velocity. In the transitionally rough regime, the friction factor varies with the Reynolds number and the roughness height, as the roughness elements begin to distort the laminar-sub layer [24, 50, 51]. The present results correspond to the fully rough regime where the viscous cycle is completely distorted by the roughness element and hence the friction factor becomes independent of the viscosity. The variation of the friction factor with the Reynolds number and the width-to-height ratio are shown in figures 6(a). Maximum resistance to the flow occurs at $w/k \approx 7$, for the lowest Reynolds number, $Re_\tau = 6,325$. This optimum flow resistance value agrees well with the DNS result of Leonardi et al. [21] and the experimental result of Furuya et al. [39] on plates roughened by wires. For all the the roughness type classes, the resistance decreases with increasing Re_τ.

A cubic polynomial curve can be fitted to the friction factor data as shown in figure 6(a). The results are in accordance with the conclusion of Saito et al. [52], who suggest that in the fully rough regime the average turbulence intensity is proportional to the friction factor. The equation for the polynomial curve is given by,

$$f = 0.005+0.01(w/k) + 0.01(w/k)^2 + 0.003(w/k)^3,\ 0.12 \lesssim w/k \lesssim 7 \tag{16}$$

A fitted cubic polynomial curve indicates a rapid rate of friction enhancement up to $w/k \approx 7$ as described in equation (16). For $w/k \gtrsim 7$, an exponential decay function can be described by fitting a curve to the data as illustrated in figure 6(a), with the exponential curve given by,

$$f = 0.02e^{\left(\frac{-(w/k)}{41.03}\right)} + 0.005,\ w/k \gtrsim 7 \tag{17}$$

Figure 6(a) demonstrates that the decay rate of the flow resistance is slow with respect to the varying w/k ratio; equation (17) indicates it is $\approx 1/41$.

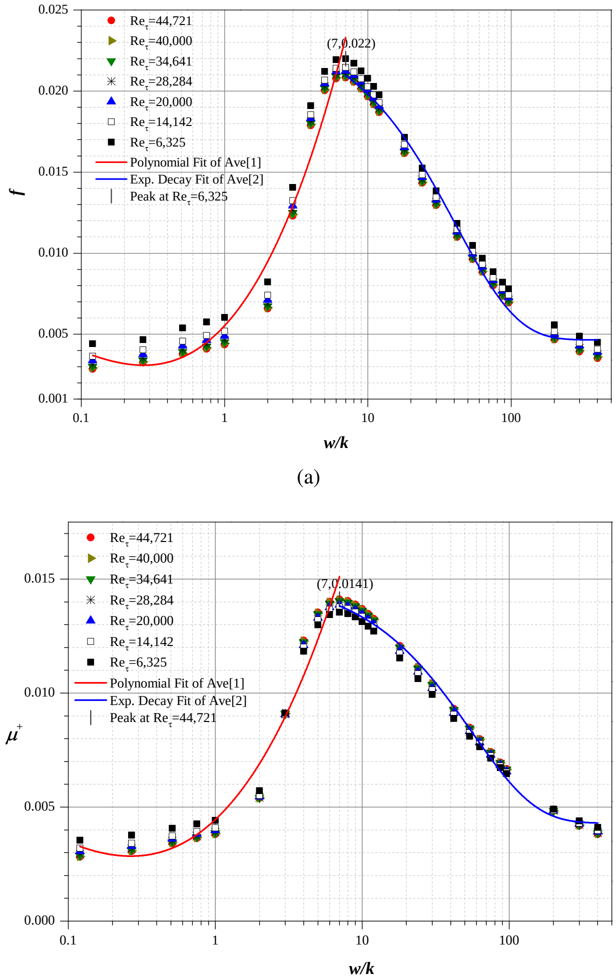

(a)

(b)

Figure 6: Scatter plots of the area-weighted average friction factor and eddy viscosity vs. w/k for a range of Reynolds numbers.

5.3. Eddy Viscosity

Eddy or turbulent viscosity μ_t is associated with the transfer of momentum caused by turbulent eddies and attributes to the local state of turbulence [53]. The eddy viscosity depends on the turbulent energy per unit mass of the fluid K, and the dissipation rate ε. The eddy viscosity μ_t is computed in a non-dimensional format which can be expressed as,

$$\mu^+ = \frac{\mu_t}{\rho\overline{U}(H/2)} \tag{18}$$

The optimal values of the w/k ratio and Reynolds number to maximise mixing enhancement can be constrained. Figure 6(b) shows that the value of μ^+ is maximised at $w/k = 7$ for highest Reynolds number at $Re_\tau = 44,721$. It is observed that the rate of eddy viscosity enhancement and decay is similar to the flow resistance. In this case the data is described by a polynomial curve given by

$$\mu^+ = 0.004{+}0.006(w/k) + 0.006(w/k)^2 + 0.001(w/k)^3,\ 0.12 \lesssim w/k \lesssim 7 \tag{19}$$

and an exponential decay equation determined to be

$$\mu^+ = 0.01e^{\left(\frac{-(w/k)}{56.13}\right)} + 0.004,\ w/k \gtrsim 7 \tag{20}$$

The normalised eddy viscosity is maximised in the range of $7 \lesssim w/k \lesssim 10$. As figure 6(b) illustrates, a polynomial curve can be fitted to the normalised eddy viscosity data for $w/k \lesssim 7$. The eddy viscosity immediately enhances up to $w/k \approx 7$ and decay exponentially at a rate of $\approx 1/56$ order of magnitude. For $w/k \lesssim 1$, the value of μ^+ decreases with increasing Reynolds number. For the intermediate type roughness, or $w/k = 3$, μ^+ becomes independent of the Reynolds number. As the flow separates and reattaches in the bed at $w/k = 7$, the eddy viscosity begins to change behaviour and increases with increasing Reynolds number. This phenomenon continues up to $w/k \approx 200$ where μ^+ once again becomes independent of the Reynolds number behaviour inclusive to the intermediate type roughness behaviour. For $w/k > 201$, μ^+ starts to decrease with an increasing Reynolds number in a similar manner observed for the d-type roughness, as the width expands towards the smooth wall limit.

6. Discussion

The new results confirm that the optimum spacing of roughness elements to maximise friction and eddy viscosity within the flow occurs at $w/k = 7$. The rate of turbulence enhancement increases rapidly up to this critical spacing and the rate of perturbation decay is slow thereafter, such that the effect of turbulence perturbation does not change significantly with the increasing aspect ratio. In turbulent pipe flows it normally takes around 100 pipe diameters for the velocity profile to become fully developed [54, 55], and this value is similar to the modelled roughness case here, in which the flow does not becomes fully developed until a distance of about 100 roughness heights downstream of a roughness element.

Okamoto et al. [40] concluded that optimal heat transfer occurs when the turbulence of the free stream is maximised. Similarly, Ryu et al. [56] found that the maximum heat transfer occurs when the flow resistance attains its maximum value. The conditions associated with optimum turbulence enhancement and the flow resistance in the present work suggest, therefore, that heat transfer enhancement is maximised during flow over roughness elements with spacing $w/k \approx 7$, but that close to optimal transfer can occur with much wider roughness spacings. This result may guide efforts to optimise heat transfer in engineering applications. It should be noted, however, that the optimal ratio of obstacle to flow height has not been constrained here: this question awaits further work.

The current results have implications in turbulent particle-laden flows of engineering and geological interest with lower rough boundaries. Seeding particles in the flow is still used as a heat transfer augmentation technique in heat-exchangers and fluidized beds [57, 58]. Classical mixing theory describes the turbulent diffusion of particulate material using an eddy diffusivity (which is proportional to the eddy viscosity, as described above [44, 59]). The enhancement of the eddy viscosity by surface roughness, suggests effective mixing and entrainment of the particles within the channel. Therefore, it would be anticipated that at $w/k \approx 7$ the dispersion and fluctuating velocities of particles is maximally modified, which this leads to an increase in the mean distribution of the particles throughout the channel.

7. Conclusions

We report the results from a RANS-based numerical modelling study of flow over lower boundary roughness elements, conducted over a wide range of Reynolds numbers. A critical width-to-height ratio of $w/k \approx 7$ is confirmed to be associated with maxima in each of flow resistance and eddy viscosity for over-passing flow. A linear rate of turbulence enhancement is seen up to $w/k = 7$, followed by an exponential rate of perturbation decay beyond this critical ratio, with no significant dependence on flow Reynolds number. The results have implications for the optimised engineering designs to enable maximum enhancement of heat transfer. Flow over erosional roughness is a source of turbulence generation for turbidity currents, but further work to constrain the interplay between drag enhancement and particle diffusion is required to clarify the implications for flow propagation.

Acknowledgements

This research was funded by the Turbidites Research Group industry consortium (Anadarko, BG, BHP Billiton, BP, ConocoPhillips, Maersk, Marathon, Nexen, Statoil, Tullow and Woodside.)

References

[1] S. A. Lawson, A. A. Thrift, K. A. Thole, A. Kohli, Heat transfer from multiple row arrays of low aspect ratio pin fins, International Journal of Heat and Mass Transfer 54 (2011) 4099 – 4109.

[2] R. Webb, E. Eckert, Application of rough surfaces to heat exchanger design, International Journal of Heat and Mass Transfer 15 (1972) 1647 – 1658.

[3] H. Sun, M. Faghri, Effect of surface roughness on nitrogen flow in a microchannel using the direct simulation monte carlo method, Numerical Heat Transfer, Part A: Applications 43 (2003) 1–8.

[4] J. Milnes, A. Burns, D. Drikakis, Computational modelling of the hypervapotron cooling technique, Fusion Engineering and Design 87 (2012) 1647 – 1661.

[5] S. Liu, M. Sakr, A comprehensive review on passive heat transfer enhancements in pipe exchangers, Renewable and Sustainable Energy Reviews 19 (2013) 64 – 81.

[6] K. Yau, J. Cooper, J. Rose, Effect of fin spacing on the performance of horizontal integral-fin condenser tubes., Journal of Heat Transfer 107 (1985) 377 – 383.

[7] B. Young, B. Vliet, The effect of surface roughness on fluid-to-particle mass transfer in a packed adsorber bed, International Journal of Heat and Mass Transfer 31 (1988) 27 – 34.

[8] J. Millward-Hopkins, A. Tomlin, L. Ma, D. Ingham, M. Pourkashanian, Estimating aerodynamic parameters of urban-like surfaces with heterogeneous building heights, Boundary-Layer Meteorology 141 (2011) 443–465.

[9] J. T. Eggenhuisen, W. D. McCaffrey, The vertical turbulence structure of experimental turbidity currents encountering basal obstructions: implications for vertical suspended sediment distribution in non-equilibrium currents, Sedimentology 59 (2012) 1101–1120.

[10] I. P. Castro, A. Segalini, P. H. Alfredsson, Outer-layer turbulence intensities in smooth- and rough-wall boundary layers, Journal of Fluid Mechanics 727 (2013) 119–131.

[11] J. Tsikata, M. Tachie, Adverse pressure gradient turbulent flows over rough walls, International Journal of Heat and Fluid Flow 39 (2013) 127 – 145.

[12] J. H. Lee, H. J. Sung, P.-A. Krogstad, Direct numerical simulation of the turbulent boundary layer over a cube-roughened wall, Journal of Fluid Mechanics 669 (2011) 397 – 431.

[13] V. Roussinova, R. Balachandar, Open channel flow past a train of rib roughness, Journal of Turbulence 12 (2011) 1–17.

[14] P. Burattini, S. Leonardi, P. Orlandi, R. Antonia, Comparison between experiments and direct numerical simulations in a channel flow with roughness on one wall, Journal of Fluid Mechanics 600 (2008) 403 – 26.

[15] D. Ryu, D. Choi, V. Patel, Analysis of turbulent flow in channels roughened by two-dimensional ribs and three-dimensional blocks. part ii: Heat transfer, International Journal of Heat and Fluid Flow 28 (2007) 1112 – 1124.

[16] J. Cui, V. C. Patel, C.-L. Lin, Large-eddy simulation of turbulent flow in a channel with rib roughness, International Journal of Heat and Fluid Flow 24 (2003) 372 – 388.

[17] A. Ashrafian, H. I. Andersson, The structure of turbulence in a rod-roughened channel, International Journal of Heat and Fluid Flow 27 (2006) 65 – 79.

[18] P.-A. Krogstad, H. Andersson, O. Bakken, A. Ashrafian, An experimental and numerical study of channel flow with rough walls, Journal of Fluid Mechanics 530 (2005) 327 – 52.

[19] P.-A. Krogstad, R. Antonia, L. Browne, Comparison between rough- and smooth-wall turbulent boundary layers, Journal of Fluid Mechanics 245 (1992) 599 – 617.

[20] S. Leonardi, I. P. Castro, Channel flow over large cube roughness: a direct numerical simulation study, Journal of Fluid Mechanics 651 (2010) 519–539.

[21] S. Leonardi, P. Orlandi, R. Smalley, L. Djenidi, R. Antonia, Direct numerical simulations of turbulent channel flow with transverse square bars on one wall, Journal of Fluid Mechanics 491 (2003) 229 – 38.

[22] L. Djenidi, R. Elavarasan, R. A. Antonia, The turbulent boundary layer over transverse square cavities, Journal of Fluid Mechanics 395 (1999) 271–294.

[23] M. Tachie, D. Bergstrom, R. Balachandar, Rough wall turbulent boundary layers in shallow open channel flow, Transactions of the ASME. Journal of Fluids Engineering 122 (2000) 533 – 41.

[24] J. Jimenez, Turbulent flows over rough walls, Annual Review of Fluid Mechanics 36 (2004) 173 – 196.

[25] R. Antonia, L. Djenidi, On the outer layer controversy for a turbulent boundary layer over a rough wall, IUTAM Symposium on The Physics of Wall-Bounded Turbulent Flows on Rough Walls, Springer Netherlands 22 (2010) 77–86.

[26] V. Chow, Te, Open-channel hydraulics, McGraw-Hill (1959).

[27] A. E. Perry, W. H. Schofield, P. N. Joubert, Rough wall turbulent boundary layers, Journal of Fluid Mechanics 37 (1969) 383–413.

[28] J. Nikuradse, Stromungsgesetze in rauhen rohren, Forschungsheft Arb. Ing.-Wes. 361 (1933).

[29] S. Leonardi, P. Orlandi, L. Djenidi, R. Antonia, Structure of turbulent channel flow with square bars on one wall, International Journal of Heat and Fluid Flow 25 (2004) 384 – 392.

[30] S. Leonardi, P. Orlandi, R. A. Antonia, Properties of d- and k-type roughness in a turbulent channel flow, Physics of Fluids (1994-present) 19 (2007) –.

[31] I. Tani, Turbulent boundary layer development over rough surfaces, Perspectives in Turbulence Studie, Springe (1987) 223–249.

[32] I. P. Castro, Rough-wall boundary layers: mean flow universality, Journal of Fluid Mechanics 585 (2007) 469–485.

[33] P. Orlandi, S. Leonardi, R. A. Antonia, Turbulent channel flow with either transverse or longitudinal roughness elements on one wall, Journal of Fluid Mechanics 561 (2006) 279–305.

[34] A. Ashrafian, H. I. Andersson, M. Manhart, {DNS} of turbulent flow in a rod-roughened channel, International Journal of Heat and Fluid Flow 25 (2004) 373 – 383.

[35] C. K. Rao, J. J. C. Picot, The effect of turbulence promoters on heat and momentum transfer for air flow in an annulus, Proceedings of 4th International Heat Transfer Conference, (1970) 1–12.

[36] R. Webb, E. Eckert, R. Goldstein, Heat transfer and friction in tubes with repeated-rib roughness, International Journal of Heat and Mass Transfer 14 (1971) 601 – 617.

[37] K. Ichimiya, Effects of several roughness elements on an insulated wall for heat transfer from the opposite smooth heated

surface in a parallel plate duct, Journal of Heat Transfer (Transcations of the ASME (American Society of Mechanical Engineers), Series C);(United States) 109 (1987).
[38] T.-M. Liou, J.-J. Hwang, S.-H. Chen, Simulation and measurement of enhanced turbulent heat transfer in a channel with periodic ribs on one principal wall, International Journal of Heat and Mass Transfer 36 (1993) 507 – 517.
[39] Y. Furuya, M. Miyata, H. Fujita, Turbulent boundary layer and flow resistance on plates roughened by wires, Transactions of the ASME. Series I, Journal of Fluids Engineering 98 (1976) 635 – 44.
[40] S. Okamoto, S. Seo, K. Nakaso, I. Kawai, Turbulent shear flow and heat transfer over the repeated two-dimensional square ribs on ground plane, Journal of Fluids Engineering 115 (1993) 631–637.
[41] ANSYS, CFX v14 Help Manuals, Solver Theory, 2011. doi:www.ansys.com/cfx.
[42] F. R. Menter, M. Kuntz, R. Langtry, Ten Years of Industrial Experience with the SST Turbulence Model, volume 4, Begell House, Inc, 2003, pp. 625–632.
[43] T. Esch, F. R. Menter, Heat Transfer Predictions Based on Two-Equation Turbulence Models with Advanced Wall Treatment, Begell House, 2003, pp. 633–640.
[44] F. R. Menter, Two-equation eddy-viscosity turbulence models for engineering applications, AIAA Journal 32 (1994) 1598–1605.
[45] C. G. Speziale, S. Sarkar, T. B. Gatski, Modelling the pressure strain correlation of turbulence: an invariant dynamical systems approach, Journal of Fluid Mechanics 227 (1991) 245–272.
[46] B. E. Launder, Second-moment closure: present and future?, International Journal of Heat and Fluid Flow 10 (1989) 282–300.
[47] K. Hanjalic, B. E. Launder, Fully developed asymmetric flow in a plane channel, Journal of Fluid Mechanics 51 (1972) 301–335.
[48] S. Leonardi, F. Tessicini, P. Orlandi, R. Antonia, Direct numerical and large-eddy simulations of turbulent flows over rough surfaces, AIAA Journal 44 (2006) 2482 – 2487.
[49] P. R. Bandyopadhyay, Rough-wall turbulent boundary layers in the transition regime, Journal of Fluid Mechanics 180 (1987) 231–266.
[50] H. Schlichting, K. Gersten, Boundary-Layer Theory, Physic and astronomy, MacGraw-Hill, 2000.
[51] A. Busse, N. D. Sandham, Parametric forcing approach to rough-wall turbulent channel flow, Journal of Fluid Mechanics 712 (2012) 169–202.
[52] N. Saito, D. I. Pullin, M. Inoue, Large eddy simulation of smooth-wall, transitional and fully rough-wall channel flow, Physics of Fluids 24 (2012) 075103.
[53] P. Nielsen, I. A. Teakle, Turbulent diffusion of momentum and suspended particles: A finite-mixing-length theory, Physics of Fluids 16 (2004) 2342.
[54] R. Patel, A note on fully developed turbulent flow down a circular pipe, Aeronautical Journal 78 (1974) 93–97.
[55] K. Lien, J. Monty, M. Chong, A. Ooi, The entrance length for fully developed turbulent channel flow, in: 15th Australasian Fluid Mechanics Conference, The University of Sydney, Australia, 2004.
[56] D. Ryu, D. Choi, V. Patel, Analysis of turbulent flow in channels roughened by two-dimensional ribs and three-dimensional blocks. part ii: Heat transfer, International Journal of Heat and Fluid Flow 28 (2007) 1112 – 1124.
[57] E. E. Michaelides, Heat transfer in particulate flows, International Journal of Heat and Mass Transfer 29 (1986) 265 – 273.
[58] K. Rajan, S. Srivastava, B. Pitchumani, K. Dhasandhan, Experimental study of thermal effectiveness in pneumatic conveying heat exchanger, Applied Thermal Engineering 28 (2008) 1932 – 1941.
[59] T.-H. Shih, W. W. Liou, A. Shabbir, Z. Yang, J. Zhu, A new k-ε eddy viscosity model for high reynolds number turbulent flows, Computers & Fluids 24 (1995) 227 – 238.